Role of sidewall diffusion in GaAs nanowire growth: A first-principles study

Volker Pankoke, Sung Sakong,* and Peter Kratzer
Fakultät für Physik and Center for Nanointegration (CENIDE), Universität Duisburg-Essen, Lotharstr. 1, 47048 Duisburg, Germany
(Received 2 July 2012; published 15 August 2012)

The molecular processes during the growth of GaAs nanowires in molecular beam epitaxy (MBE) are studied from first principles. For the wurtzite crystal structure of GaAs, which is formed exclusively in nanowire growth, potential energy surfaces for sidewall diffusion of Ga, As, and GaAs surface species are calculated using density functional theory. We compare materials transport on type-I and -II nanowires (with $\{10\bar{1}0\}$ and $\{11\bar{2}0\}$ facets of wurtzite GaAs, respectively) and discuss its role for materials supply to the growth zone at the nanowire tip. On the sidewalls of type-II nanowires, the diffusion barrier for Ga along the growth direction is particularly low, only 0.30 eV compared to 0.60 eV on type-I nanowires. For As adatoms, the corresponding diffusion barriers are 0.64 eV and 1.20 eV, respectively, and hence higher than for Ga adatoms. The GaAs molecule formed by the chemical surface reaction of Ga and As finds very stable binding sites on type-II sidewalls where it inserts itself into a chemical bond between surface atoms, triggering radial growth. In contrast, on type-I nanowires the GaAs molecule adsorbed with the As end towards the surface has a low diffusion barrier of 0.50 eV. Together with our previous finding that the gold particle at the nanowire tip is efficient in promoting dissociative adsorption of As_2 molecules, we conclude that the influx of Ga adatoms from sidewall diffusion is very important to maintain stoichiometric growth of GaAs nanowires, in particular when a large V-III ratio is used in MBE.

DOI: 10.1103/PhysRevB.86.085425 PACS number(s): 31.15.A−, 81.05.Ea, 81.07.Gf, 68.35.Fx

I. INTRODUCTION

The growth of one-dimensional semiconductor nanostructures on a substrate by molecular beam epitaxy (MBE) or chemical vapor deposition has been studied since the 1960s. By using nanoparticles acting as catalyst that promotes the growth via the vapor liquid solid (VLS) mechanism,[1] experimentalists have a well-established growth technique. In recent years, this method has been complemented by the so-called self-catalyzed growth[2–4] on a substrate with a thin native oxide layer without the need for an external catalyst. The interest in the controlled fabrication of group III-V semiconductor nanowires (NWs) with specific properties is still strong, due to their potential use in electronic or optoelectronic devices, such as wrapped-gate field effect transistors,[5] resonant tunneling diodes[6] with potential use as single-photon emitters, or solar cells.[7] By varying the temperature or the flux of one of the constituents, it is possible to tune the NW properties. These possibilities include, for example, the growth of core-shell structures,[7,8] or the controlled switching between wurtzite and zinc-blende wire segments in the NWs (Refs. 6 and 9). For a better understanding of the effect of different growth conditions, an atomistic description of growth is necessary.

From an atomistic perspective, the material incorporated into the nanowire may be supplied via three different routes: As the first possibility, material is adsorbed on the NW sidewalls directly from the molecular beam and diffuses to the NW tip, where it is incorporated at the growth zone. As the second possibility, it has been debated in the literature if part of the material comes from the substrate,[10] where adatoms from the vapor phase are adsorbed and diffuse to the NW footing. It has been argued based on experiments for dense arrays of InAs NWs that this source of material is important.[11] However, analysis of recent experiments on GaAs and InAs/InP wires has led to the conclusion that mass transport from the substrate may be absent, or even contributes negatively to the overall material balance.[12,13] As the third possibility, impingement of atoms or molecules from the vapor phase at the catalyst may act as a continuous materials supply. Moreover, the gold particle, which is often used as a catalyst, has the ability to store Ga atoms by alloy formation, and, albeit to a smaller extent, to store arsenic by forming surface chemical species.[14] In the present paper, we focus on surface diffusion on the NW sidewalls, which is essential for the first two supply routes discussed above. We stress that these processes are relevant both for the Au-catalyzed and for the self-catalyzed NW growth.

A quantitative analysis of the material transport on the NW side facets has been hampered by an insufficient knowledge of the atomic structure of the surfaces and the species of the transported material. In comparison to experiments of MBE growth of zinc-blende GaAs films,[15] it appears that the NW sidewalls are formed by the facets with the lowest growth speed. For wurtzite GaAs NWs, however, data of facet growth speed are unavailable, and hence conclusions about the expected sidewall facets cannot be drawn. The NW growth direction appears to be predetermined by intrinsic features of the crystal structures: along the preferred $[\bar{1}\bar{1}\bar{1}]$ growth direction in zinc blende, the crystal consists of a sequence of GaAs layers with hexagonal atomic structure stacked in an ABC stacking; similarly, along the [0001] growth direction of wurtzite, such GaAs layers in an AB stacking sequence are found. Scanning electron microscopy investigations show a hexagonal cross section of the III-V NWs (Ref. 16), where the sidewalls of the wurtzite segments are supposed to have $\{10\bar{1}0\}$ surfaces (type I)[17,18] or $\{11\bar{2}0\}$ surfaces (type II).[13] According to density-functional calculations[19] both orientations have very similar surface energies for GaAs NWs. For zinc-blende NWs, the $\{1\bar{1}0\}$ facets (being equivalent to $\{110\}$) clearly have the lowest surface energy according to the calculations by us[19] and other researchers.[20,21] In this paper, we present results of our calculations for the diffusion on the GaAs wurtzite surfaces in order to complement our understanding of sidewall diffusion.

 ©2012 American Physical Society

For zinc-blende GaAs(110), analogous results are described in the literature.[22,23]

Concerning the species responsible for materials transport, some clues can be obtained from molecular-beam epitaxy on the most-studied GaAs(001) surface. In principle, the species could be Ga or As adatoms, or GaAs or As_2 molecules. Since the lifetime of arsenic molecules on GaAs(001) is known to be very short,[24] As_2 diffusion is not considered here. Arsenic is assumed to diffuse as an atom, and to combine to a GaAs molecule when encountering a Ga adatom, or desorb as an As_2 molecule after recombining with another As adatom. For the GaAs(001) surface, the diffusion barriers for both Ga (Ref. 25) and As (Refs. 26 and 27) adatoms were obtained from density-functional calculations. Analogously, diffusion barriers for Ga on various reconstructed GaAs(111) and (110) surfaces have been calculated recently.[23] Experimental studies of surface morphology are usually interpreted in terms of Ga diffusion. However, in simple solid-on-solid growth models that have been parametrized to match experimental observations, diffusion of GaAs molecules in addition to diffusion of Ga atoms has also been considered.[28] In this work, we use density-functional theory (DFT) to calculate the potential energy surfaces (PESs) that govern diffusion on the GaAs wurtzite $\{10\bar{1}0\}$ and $\{11\bar{2}0\}$ surfaces for Ga and As adatoms, as well as GaAs molecules. The following section introduces the methods used for our calculations and for the analysis of the data. In Sec. III, we present the calculated PESs and discuss the significance of the results. The consequences for the nanowire growth are discussed in Sec. IV, followed by a concluding section.

II. METHODOLOGY

The sidewall facet of NW with a diameter of several hundred nm is large enough to be treated as an infinite surface, because the influence of edges on the electronic structure becomes negligible. Therefore, in order to simulate NW sidewalls, the slab approach, as commonly used in surface calculations, is appropriate. The $\{10\bar{1}0\}$ and $\{11\bar{2}0\}$ facets of wurtzite NWs are modeled by periodic slabs which consist of eight (in case of the $\{1\bar{1}00\}$ orientation) or seven (in case of the $\{11\bar{2}0\}$ orientation) GaAs layers (see Fig. 1). Above the surfaces a vacuum spacing of at least 8 Å is retained, and we take 2×2 supercells to reduce artificial interactions between the adatom and its periodic images. This leads to supercells with periodic boundary conditions containing 64 (for $\{10\bar{1}0\}$) or 56 (for $\{11\bar{2}0\}$) GaAs pairs, passivated with 16 pseudohydrogen atoms with a fractional charge on the bottom side. In the first step, the top-most five GaAs layers of the clean surfaces without an adatom are completely relaxed. In the second step, the PESs are mapped out for an adatom or a molecule on top of the surface. The adatom is positioned on a 7×8 grid over the surface, keeping its x and y coordinates fixed and minimizing the forces in the z direction to obtain the relaxed adatom position. In the case of the GaAs molecule, an additional Ga atom is placed above an As adatom. The As atom position is fixed laterally as described above, while the Ga atom is free to relax in every direction. At each mesh point, the positions of the low-most 24 GaAs pairs for $\{10\bar{1}0\}$ (16 pairs for $\{11\bar{2}0\}$) and of the H atoms are fixed at their slab

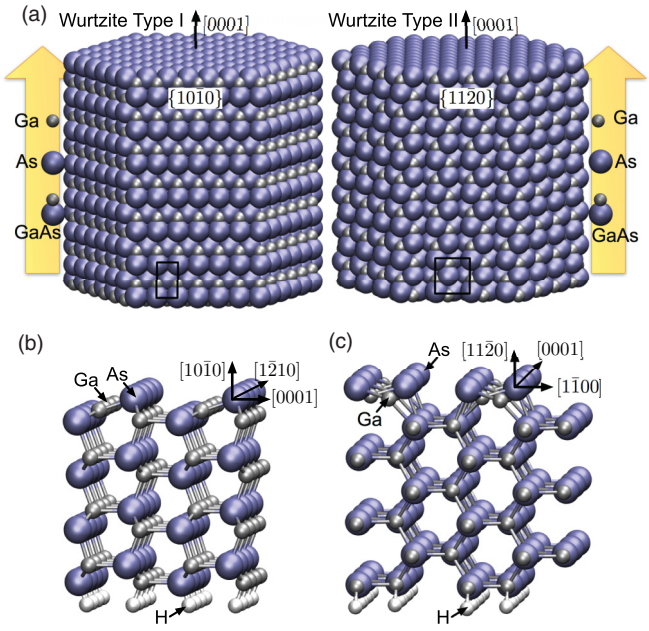

FIG. 1. (Color online) (a) Scheme of adatom diffusion along type-I and -II wurtzite GaAs nanowire sidewalls and corresponding slabs (in side view) with (b) $\{10\bar{1}0\}$ and (c) $\{11\bar{2}0\}$ surfaces. The large, dark (blue) balls are As atoms and the small, light (silver) balls are Ga atoms. The bottom surface is passivated by pseudohydrogen atoms (small, white balls).

optimized positions, so that the five top-most layers of GaAs pairs are treated as a model for the surface and are further relaxed with an adatom or a molecule.

At each grid point, a DFT calculation has been performed using a basis set of plane waves for the electronic wave functions, as implemented in the Vienna *Ab-initio* Simulation Package [VASP (Ref. 29)]. The $4s$ and $4p$ electrons of Ga and As are treated as valence electrons, and the remaining core electrons are described using the projector-augmented-wave method (PAW).[30] The pseudohydrogen atoms used for passivation have 0.75 or 1.25 elementary charges. The k-point mesh is created using the Monkhorst-Pack[31] scheme with a $4 \times 4 \times 2$ resolution. The exchange-correlation potential is approximated with the Perdew-Burke-Ernzerhof approach (PBE).[32] An energy cutoff of 150 eV of the plane wave basis is found to be sufficient.

The PESs are constructed by interpolating the discrete grid data. The energies are presented with respect to the energy of the clean surface, and of a free species in the gas phase, E_X. Here, E_X may represent E_{Ga}, the energy of a free, spin-polarized Ga atom, or E_{As}, half the energy of a gas-phase As_2 molecule, or E_{GaAs}, the energy of a free GaAs molecule, respectively.

III. POTENTIAL ENERGY SURFACES

Adatoms on the NW facets have to migrate along the [0001] direction of the hexagonal wurtzite NW to reach the growth zone (the interface with the Au particle in case of Au-catalyzed growth) and get incorporated into the structure. Potential energy surfaces are calculated for two different sidewall facets, wurtzite $\{10\bar{1}0\}$ and $\{11\bar{2}0\}$, and for three different kinds of

TABLE I. Potential energies at local minima and saddle points on the $\{10\bar{1}0\}$ facet for Ga, As, and GaAs adatoms. The adsorption energy gain is defined with respect to the energy of atomic Ga, gas-phase As_2, and GaAs molecules. The negative sign means energy gain by adsorption. The barrier is the activation energy for the saddle point with respect to the initial minimum A_j.

Adatom	Minima (eV)		Saddle points (eV)		Barrier (eV)
Ga	A_1	−2.34	$T_1(A_1 \to A_1)$	−1.74	0.60
			$T_2(A_1 \to A_1)$	−2.24	0.10
			$T_3(A_1 \to A_1)$	−2.31	0.03
As	A_1	−2.10	$T_1(A_1 \to A_2)$	−0.88	1.22
	A_2	−1.93	$T_2(A_2 \to A_1)$	−1.54	0.39
	A_3	−1.68	$T_3(A_1 \to A_3)$	−1.58	0.52
GaAs	A_1	−2.91	$T_1(A_1 \to A_2)$	−2.53	0.38
	A_2	−2.74	$T_2(A_2 \to A_3)$	−2.40	0.34
			$T_4(A_2 \to A_2)$	−2.64	0.10
	A_3	−2.52	$T_3(A_3 \to A_1)$	−2.46	0.06

adatoms and molecules, Ga, As, and GaAs. The figures are arranged in such a way that the vertical axis points into the [0001] direction, which in the case of a GaAs NW is the growth direction, and the material from the substrate should diffuse in this direction to promote growth. Minima and saddle points are labeled A_j and T_i, respectively, in the figures, and their exact energy values taken from higher resolution contour plots are listed in Tables I and II.

A. Type-I nanowire: $\{10\bar{1}0\}$ facets

Figure 2 shows the PESs of the $\{10\bar{1}0\}$ surface over an energy range of 1.5 eV, starting at the lowest minimum. The positions of the top-most Ga [small, light (silver) balls] and As [large, dark (blue) balls] atoms are superimposed on the PESs: At the $\{10\bar{1}0\}$ facet, higher-lying, tilted GaAs pairs alternate with lower-lying GaAs pairs (the latter are shown as dark gray balls in the figures).

TABLE II. Potential energies at local minima and saddle points on the $\{11\bar{2}0\}$ facet for Ga, As, and GaAs adatoms. The adsorption energy gain is defined with respect to the energy of atomic Ga, gas-phase As_2, and GaAs molecules. The barrier is the activation energy for the saddle point with respect to the initial minimum A_j.

Adatom	Minima (eV)		Saddle points (eV)		Barrier (eV)
Ga	A_1	−2.56	$T_1(A_1 \to A_1)$	−2.24	0.32
			$T_3(A_1 \to A_2)$	−2.29	0.27
	A_2	−2.37	$T_2(A_2 \to A_2)$	−2.09	0.28
			$T_4(A_2 \to A_1)$	−2.28	0.09
As	A_1	−2.45	$T_1(A_1 \to A_1)$	−1.80	0.65
			$T_3(A_1 \to A_1)$	−1.80	0.65
			$T_4(A_1 \to A_2)$	−1.70	0.75
	A_2	−2.09	$T_2(A_2 \to A_1)$	−1.80	0.29
GaAs	A_1	−3.26	$T_1(A_1 \to A_2)$	−2.56	0.70
			$T_5(A_1 \to A_4)$	−2.71	0.55
	A_2	−2.64	$T_2(A_2 \to A_3)$	−2.47	0.17
			$T_4(A_2 \to A_1)$	−2.45	0.19
	A_3	−2.55	$T_3(A_3 \to A_2)$	−2.37	0.18
	A_4	−2.73	$T_6(A_4 \to A_3)$	−2.34	0.39

For the diffusion of adatoms, we notice a maximum of the PESs for all adatoms at the topographically highest point of the surface, the upper arsenic atom row. In case of a gallium adatom (left panel of Fig. 2), the energetically favored diffusion path along [0001] leads from the minimum at A_1 over T_1 to the next A_1 minimum ($A_1 \to T_1 \to A_1$ path). The energy barrier in this direction is 0.60 eV. For a diffusion in $[1\bar{2}10]$ direction ($A_1 \to T_2 \to A_1 \to T_3 \to A_1$ path), we find an effective barrier (the largest barrier in the path) of 0.10 eV across T_2. These barriers are calculated from the results for the adsorption energies listed in Table I.

In the simplest possible treatment of activated diffusion, using transition state theory, the diffusion coefficient is given by

$$D = \frac{1}{4} a_0^2 \Gamma_0 \exp\left(-\frac{\Delta E_{\text{eff.}}}{k_B T}\right) \tag{1}$$

where $\Delta E_{\text{eff.}} = E(T_i) - E(A_j)$ is the energy barrier between the lowest minimum energy A_j and the highest saddle point T_i in the path. k_B is the Boltzmann constant and T is the temperature in Kelvin. The pre-exponential factor consists of the attempt frequency Γ_0 and the distance between two neighboring minima of the same kind a_0. For a rough estimation, one may assume Γ_0 as 1×10^{13} s^{-1}, a typical value for surface diffusion of adatoms; for a more accurate treatment, see Refs. 33 and 34. Using this rough estimation, we find effective diffusion coefficients of $D_{[0001]} = 1.87 \times 10^{-6}$ cm^2/s and $D_{[1\bar{2}10]} = 9.71 \times 10^{-4}$ cm^2/s at 800 K for the two orthogonal directions along the surface. Obviously there is a large anisotropy between the diffusion in the growth direction and the diffusion orthogonal to it.

For arsenic adatoms the energy barrier is much higher, as shown in the middle panel of Fig. 2 and Table I. The diffusion path in the [0001] direction for an arsenic adatom ($A_1 \to T_1 \to A_2 \to T_2 \to A_1$) leads over the transition point T_1 located above the Ga–As bond. From the calculated binding energy with respect to free As_2 molecules in Table I, we find an energy barrier in the [0001] direction of 1.22 eV and in the $[11\bar{2}0]$ direction of 0.52 eV. The corresponding diffusion coefficients are $D_{[1\bar{2}10]} = 2.19 \times 10^{-6}$ cm^2/s and $D_{[0001]} = 2.32 \times 10^{-10}$ cm^2/s at 800 K. The highly corrugated PES in the middle panel of Fig. 2 and the empirically known short lifetime of As at the surface[24] let us conclude that As sidewall diffusion plays a minor role in the growth of GaAs nanowires.

The right panel of Fig. 2 shows the PES of a GaAs molecule on the $\{10\bar{1}0\}$ facet. At the transition point T_2, the energy barrier is strongly reduced compared to that of arsenic adatoms and even compared to Ga adatoms. As seen from Table I, the effective barrier along [0001] direction is only 0.51 eV, which leads to a diffusion coefficient of 6.90×10^{-6}cm^2/s at 800 K along the [0001] direction. There are similar barriers of 0.45 and 0.38 eV along the $[1\bar{2}10]$ direction ($A_1 \to T_3 \to A_3 \to T_3 \to A_1$ and $A_1 \to T_1 \to A_2 \to T_4 \to A_2 \to T_1 \to A_1$ paths, respectively), and the resulting diffusion coefficient of the lower barrier path is 1.67×10^{-5} cm^2/s. At first, it appears unexpected that attaching a Ga atom to the As adatom reduces its diffusion barrier. However, Horch *et al.* experimentally observed a similar phenomenon, enhanced

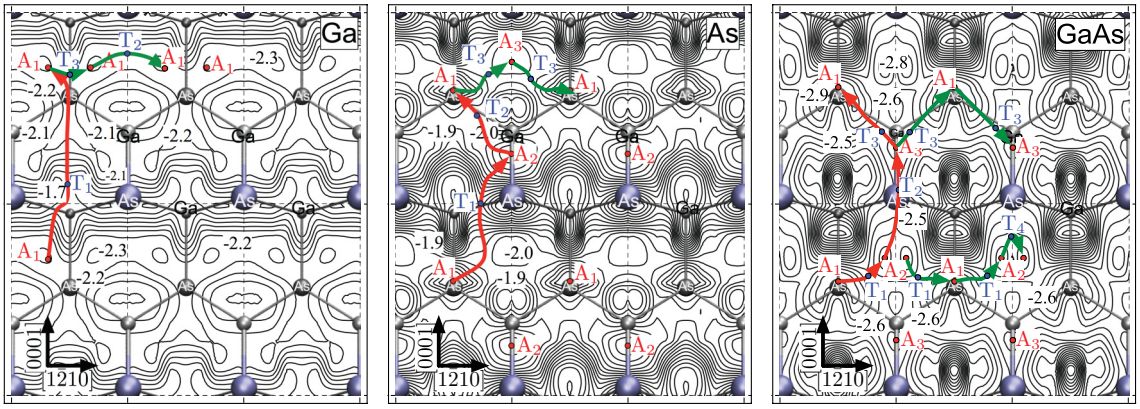

FIG. 2. (Color online) Potential energy surfaces of Ga, As, and GaAs adatoms on the sidewalls of a type-I wurtzite nanowire ($\{10\bar{1}0\}$ surface). The large, dark (blue) balls are As atoms and the small, light (silver) balls are Ga atoms in the first GaAs layer. The dark gray atoms represent Ga and As atoms in the second layer. A_i and T_i are the local energy minima and saddle points on the energy surfaces, respectively. The detailed values are listed in Table I.

self-diffusion for Pt adatoms with adsorbed hydrogen atoms.[35] Thus, in the same way the hydrogen atom decreases the diffusion barrier of Pt, the diffusion barrier of the As adatom may be decreased by the attached Ga atom. Consequently, the surface chemical reaction of Ga and As species to GaAs molecules does not impede the mass transport on type-I nanowire facets. The critical nucleus for radial growth is larger than a single GaAs unit.

B. Type-II nanowire: $\{11\bar{2}0\}$ facets

The $\{11\bar{2}0\}$ facets of wurtzite GaAs NWs display similar structural features as the $\{1\bar{1}0\}$ facets of zinc-blende NWs. The top-most layer of both surfaces consists of chains of alternating three-fold coordinated Ga and As atoms. While on the $\{1\bar{1}0\}$ facet of zinc-blende NWs these chains run across the facet diagonal to the growth direction; the chains on the $\{11\bar{2}0\}$ facets of wurtzite NWs run in the [0001] growth direction. Hence, they don't form an obstacle for materials transport towards the growth zone of the NW. In Fig. 3, the As and Ga atoms of these chains are superimposed on the PESs. The trenches between these chains contain second-layer Ga and As atoms that also form chains along the [0001] direction. The favored adsorption positions depend on the adatoms species. Gallium adatoms prefer positions in the trench between the chains, whereas arsenic adatoms preferentially adsorb on top of the chains.

For Ga diffusion, we see from the PES in the left panel of Fig. 3 that the effective energy barrier along the [0001] direction is given by the difference between the minimum A_1 and the transition point T_1, with $\Delta E_{\text{eff.}} = 0.32$ eV. The diffusion coefficient along this direction is $D_{[0001]} = 1.09 \times 10^{-4}$ cm^2/s at 800 K. For $D_{[1\bar{1}00]}$ we find 2.14×10^{-4} cm^2/s at $T = 800$ K with $\Delta E_{\text{eff.}} = E(T_4) - E(A_1) = 0.28$ eV. The binding energies of the Ga adatoms at the various sites are listed in Table II. We note that the diffusion barrier in the growth direction is somewhat lower than the corresponding barrier of 0.57 eV (Ref. 23) on the zinc-blende GaAs(110) surface, despite the very similar structural motif of Ga–As chains.

The middle panel of Fig. 3 shows the PES of an As adatom at a $\{11\bar{2}0\}$ facet. The favored adsorption positions A_1 and A_3 lie above the top-most Ga–As chain. At the $\{11\bar{2}0\}$ facet the energy barrier for As diffusion in the [0001] direction ($A_1 \rightarrow T_1 \rightarrow A_1$ path) is $\Delta E_{\text{eff.}} = 0.65$ eV, and hence lower than on the $\{10\bar{1}0\}$ facet, but still high compared to the barrier for Ga

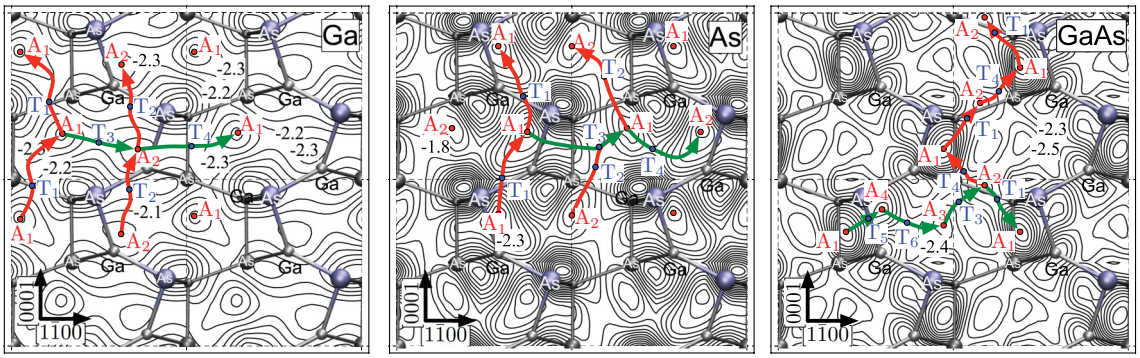

FIG. 3. (Color online) Potential energy surfaces of Ga, As, and GaAs adatoms on the sidewalls of a type-II wurtzite nanowire ($\{11\bar{2}0\}$ surface).

adatoms. Inside the trench we find a further minimum A_2 with somewhat higher energy than A_1. Hence these sites are just metastable and not relevant for the diffusivity; As adatoms at this position diffuse back onto the Ga–As chains. The diffusion coefficients at 800 K are $D_{[1\bar{1}00]} = 2.34 \times 10^{-7}$ cm^2/s and $D_{[0001]} = 9.06 \times 10^{-7}$ cm^2/s. The adsorption energies are given in Table II.

The right panel of Fig. 3 shows the PES of GaAs molecules. The binding energies of the GaAs molecule at the various sites with respect to a free GaAs molecule are summarized in Table II. The deepest minimum A_1 is found somewhat to the left or to the right of the top-most Ga–As chain. Such a behavior differs from both, the As adatoms, which migrate *on* the Ga–As chains, and from the Ga adatoms, which favor the positions in the trench between Ga–As chains. The very strong binding at the site A_1 (see Table II) is related to the fact that the As atom of the GaAs molecule inserts itself into the adjacent Ga–As bond of the Ga–As chain, resulting in a significant relaxation of the atomic structure. In the case of GaAs molecules the diffusion in the [0001] direction ($A_1 \rightarrow T_1 \rightarrow A_2 \rightarrow T_4 \rightarrow A_1 \rightarrow T_1 \rightarrow A_2 \rightarrow T_4 \rightarrow A_1$ path) leads from the A_1 minimum over the saddle point T_4 with an effective energy barrier of 0.81 eV. At 800 K, the diffusion coefficient is $D_{[0001]} = 8.89 \times 10^{-8}$cm^2/s, which is lower than the pure As result. For diffusion orthogonal to the growth direction, the path leads from A_1 over T_6, with a similar barrier height of 0.92 eV. We find a diffusion coefficient at 800 K of $D_{[1\bar{1}00]} = 6.63 \times 10^{-9}$ cm^2/s. In contrast to the results for $\{10\bar{1}0\}$ facets, the energy barrier of GaAs molecules on $\{11\bar{2}0\}$ facets is higher than for single As adatoms or Ga atoms. This finding is due to the special bonding of GaAs in the deep minimum A_1 that may act as a nucleation site for radial NW growth. Consequently, the surface chemical reaction of Ga and As species to GaAs molecules will lead to a slowing down of materials transport on this facet. We note that the situation on the $\{11\bar{2}0\}$ surface, with Ga adatoms being the most mobile species, while GaAs molecules are less mobile, is in line with the conclusions drawn from growth simulations for GaAs(001) based on the solid-on-solid model.[28]

IV. CONSEQUENCES FOR NANOWIRE GROWTH

In Table III, the diffusion constants at 800 K for the various species along the [0001] growth direction are collected. In a previous paper,[14] we have put forward the view that the arsenic species in Au-catalyzed nanowire growth is delivered mostly by direct impingement and catalytic dissociation of arsenic molecules at the Au particle, while the Ga species could originate both from direct impingement on the Au particle or from influx via sidewall diffusion. The results of the present calculations are consistent with this view; the diffusivity of As adatoms is lower than the diffusivity of Ga adatoms on the side facets of both type-I and -II NWs. At the same time, we find that Ga diffusivity on the sidewalls is very high, much higher, in fact, than on other GaAs surfaces studied so far.[23,25] In MBE experiments, typically a much larger flux of arsenic molecules, F_{As}, compared to the flux of Ga atoms, F_{Ga}, is used. Thus, it is plausible that the smaller number of Ga atoms impinging on the Au particle is complemented by a flux of Ga adatoms from the sidewalls diffusing to the growth zone to ensure stoichiometric growth.

TABLE III. Diffusion constants in cm^2/s along the [0001] direction at $T = 800$ K for the surface species Ga, As, and GaAs on NWs with type-I or -II side facets.

	Ga	As	GaAs
Type I	1.87×10^{-6}	2.32×10^{-10}	6.90×10^{-6}
Type II	1.09×10^{-4}	9.06×10^{-7}	8.89×10^{-8}

For a quantitative analysis of the materials balance, one has to distinguish various growth regimes: In one regime, the applied flux of As molecules or the kinetics at the Au particle may limit the growth speed.[2] In another regime, the influx of Ga atoms from the sidewalls could be the limiting factor. In the following, we restrict our discussion to this second regime. In an experiment, the scaling of the axial growth speed with wire diameter may be used as an indicator for this regime: If the NWs have constant radius R, the material required to lengthen the wire by a fixed amount scales quadratically with R, while the material supply by sidewall diffusion scales with the circumference, i.e., it is proportional to R. From such simple considerations, it becomes clear that the regime where material supply via sidewall diffusion is rate-limiting should be characterized by a $1/R$ scaling of the growth speed. Experimentally, such a $1/R$ dependence has been observed, e.g., for InP NWs; see Fig. 5 in Ref. 36. Other experiments on AlGaAs and GaAs NW growth[37,38] found a crossover between a $1/R^2$ dependence and a $1/R$ dependence of the NW growth speed. For arrays of InAs NWs, deviations from the $1/R$ law have been reported as well,[11] possibly due to neighboring NWs competing for the material.

In the regime where sidewall diffusion is important, our calculations corroborate the principal possibility of Ga diffusion all the way from the substrate to the wire tip: The diffusivity of Ga on the NW sidewalls is sufficiently high, and losses due to evaporation of Ga are small at typical growth temperatures due to the large adsorption energy of Ga on these facets of 2.34 to 2.56 eV; see Tables I and II. This ensures that temperatures as high as 1000 K can be employed in catalyst-free MBE growth of GaAs NW without observing any tapering of the NWs (Ref. 2).

First we discuss arsenic-limited growth. If the Ga beam is directed towards the substrate under an angle $\theta \neq 0$ with the substrate normal, the Ga atoms impinging on the NW sidewalls will in many cases already be sufficient to ensure growth of stoichiometric GaAs. Note that excess Ga atoms may be "stored" in the Au nanoparticle by forming a AuGa alloy, while the capability to "store" As atoms is very limited due to the small low-pressure solubility of As in Au. In a very simple model, illustrated in Fig. 4, arsenic molecules are assumed to stick only to the hemispherical particle at the NW tip, while Ga atoms may stick to both the particle surface and a cylindrical region of length L near the NW tip that is geometrically accessible. For stoichiometric growth, we need

$$[\pi R^2(1+\cos\theta) + \pi RL]F_{\mathrm{Ga}} = 2\pi R^2 F_{\mathrm{As}}, \qquad (2)$$

which yields $L = R(2F_{\mathrm{As}}/F_{\mathrm{Ga}} - 1 - \cos\theta)$. For a NW of height H with perfect side facets, all Ga atoms impinging

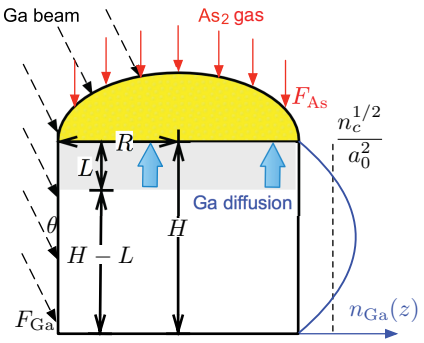

FIG. 4. (Color online) Schematics of a simple growth model with Ga atom impingement onto the sidewalls. Ga atoms impinging in the gray-shaded collection zone are required to diffuse to the metal-nanowire boundary to maintain stoichiometric growth. Sidewall nucleation is likely where the stationary concentration $n_{\mathrm{Ga}}(z)$ exceeds a critical value.

above the height $H - L$ are required diffuse to the triple-phase boundary to ensure stoichiometric growth.

For the simulation of general NW growth, including Ga-limited growth conditions, a numerical solution of the one-dimensional diffusion equation along the sidewall

$$\frac{\partial n_{\mathrm{Ga}}}{\partial t}(z,t) = D^{\mathrm{Ga}}_{[0001]} \frac{\partial^2 n_{\mathrm{Ga}}}{\partial z^2}(z,t) + F_{\mathrm{Ga}} - N(n_{\mathrm{Ga}}) \tag{3}$$

is sought for. Here, z is the coordinate along the growth direction, $n_{\mathrm{Ga}}(z,t)$ is the concentration of Ga adatoms, and $N(n_{\mathrm{Ga}})$ includes the Ga loss through sidewall nucleation and island growth. The Ga loss on NW sidewalls is relatively small; thus a stationary solution for absorbing boundary conditions at both the NW tip and footing, neglecting $N(n_{\mathrm{Ga}})$ contributions, is obtained as

$$n_{\mathrm{Ga}}(z) = \frac{F_{\mathrm{Ga}} \sin\theta}{4D}[(H/2)^2 - (z - H/2)^2]. \tag{4}$$

Then the adatom concentration vanishes near the NW tip, $n_{\mathrm{Ga}}(H) = 0$, and is maximal at half of the NW height (see blue curve in Fig. 4).

In some experiments of Au-catalyzed NW growth, e.g., in Ref. 39, a tapering of the wires is observed under prolonged growth. This has been ascribed to a shrinking of the particle at the NW tip due to insufficient supply of Ga. Since the evaporation loss is small, the major loss mechanism (for axial growth) is nucleation on the sidewalls triggering radial growth of the NWs. It has been observed experimentally[40] that the radial growth rate is sensitive to both the As flux and the molecular arsenic species used in MBE (more reactive As_2 or less reactive As_4 molecules). To estimate if nucleation takes place under given conditions, we assume that two Ga adatoms at neighboring sites are required to allow for adsorption of As_2, similar to the findings on GaAs(001) (Ref. 25). Nucleation is likely if the squared Ga adatom concentration exceeds some critical value, $a_0^4 n_{\mathrm{Ga}}^2(z) > n_c$, where n_c is a dimensionless number of order unity that depends on the molecular species of arsenic and the flux used. Since the growth zone at the NW tip is a sink for Ga adatoms, there is a denuded zone of height $l(T)$ right below the NW tip where nucleation is unlikely. Equating $a_0^4 n_{\mathrm{Ga}}^2(l) = n_c$, where the Ga density is taken from Eq. (4), we obtain

$$l(T) = \frac{H}{2}\left(1 - \sqrt{1 - \frac{16 n_c^{1/2} D^{\mathrm{Ga}}_{[0001]}(T)}{H^2 a_0^2 F_{\mathrm{Ga}} \sin\theta}}\right). \tag{5}$$

Using our calculated Ga diffusion constant $D^{\mathrm{Ga}}_{[0001]} = 1.87 \times 10^{-6}\ \mathrm{cm}^2/\mathrm{s}$ at $T = 800\mathrm{K}$ on the $(10\bar{1}0)$ surface, a NW height of $H = 8 \times 10^{-3}\mathrm{cm}$, and a typical value $a_0^2 F_{\mathrm{Ga}} \sin\theta = 1$ monolayer/s for the flux, a value of $l = 2.15 \times 10^{-3}$ cm is obtained. In the early stages of growth, as long as the NW is shorter than l, sidewall nucleation will not take place, and the materials transport by Ga sidewall diffusion is very efficient. For longer, but thin wires, nucleation and island growth on the sidewalls will consume some Ga atoms before they can reach the growth zone. One may distinguish two cases: If $l > L$, there is sufficient Ga supply to consume the whole arsenic flux sticking at the metal particle. For $l < L$, a Ga-limited regime is reached where unused As_2 molecules will desorb from the metal particle. Tapering may set in if $l < L$, because nucleation on the sidewalls and radial growth will diminish the Ga supply for axial growth. Thus, the tapering occurs in a regime of relatively fast NW axial growth due to a high V-III ratio (= large L) but reduced temperature [= small $l(T)$].

V. CONCLUSIONS

The potential energy surfaces governing diffusion on the sidewalls of GaAs wurtzite nanowires have been determined from DFT calculations. The topography of the PESs is found to be similar to those for the group-III-nitrides GaN (Ref. 41 and 42) and AlN (Ref. 43), for which the corresponding wurtzite facets are accessible on macroscopic samples. In summary, we find that Ga adatoms are able to diffuse over large distances on the sidewalls of GaAs nanowires, while adsorbed As atoms have a much shorter diffusion length. Moreover, the Ga diffusion barriers on the wurtzite surfaces are comparable or even smaller than the barrier on zinc-blende GaAs(110) (Ref. 23), and thus the diffusivity of Ga on the NW sidewalls is higher than for any other GaAs facets where experimental[44] or theoretical[23,25] studies are available so far. Taking into account our previous result[14] that the Au particle at the nanowire tip is very efficient in promoting dissociative adsorption of As_2 molecules, we conclude that the influx of Ga from the sidewalls to the growth zone at the triple-phase boundary is very important to maintain growth of stoichiometric GaAs, in particular in MBE using large V-III ratio. Under these conditions, Ga atoms from a large area of the nanowire sidewall will be collected to feed the growth. However, if nucleation on the sidewalls and radial growth sets in, the availability of Ga atoms from the sidewalls may limit the axial growth speed. The strong binding site found in our calculations for GaAs molecules on the $\{11\bar{2}0\}$ facets may facilitate nucleation on these sidewalls. Consequently, on nanowires with both type-I and -II facets coexisting, the $\{11\bar{2}0\}$ facets may grow out and eventually disappear. In a previous study,[19] we had argued that, due to the very similar surface energies of wurtzite GaAs$\{10\bar{1}0\}$ and $\{11\bar{2}0\}$, one would expect to find both facets on the wurtzite GaAs nanowires. The kinetic arguments presented above thus provide an explanation why wurtzite nanowires grown to their full length predominately display

$\{10\bar{1}0\}$ side facets. Furthermore, the information about the sidewall diffusivity obtained from our calculations could help to clarify the scope of different growth regimes where either the influx of material to the growth zone or the rate of nucleation at the triple-phase boundary is limiting the rate of axial growth.

ACKNOWLEDGMENTS

We acknowledge the Center for Computational Sciences and Simulation (CCSS) of the University Duisburg-Essen for the computer time and the Deutsche Forschungsgemeinschaft DFG for the financial support through the Project KR 2057/5-1.

*sung.sakong@uni-due.de

[1] R. S. Wagner and W. C. Ellis, Appl. Phys. Lett. **4**, 89 (1964).
[2] C. Colombo, D. Spirkoska, M. Frimmer, G. Abstreiter, and A. Fontcuberta i Morral, Phys. Rev. B **77**, 155326 (2008).
[3] B. Mandl, J. Stangl, E. Hilner, A. A. Zakharov, K. Hillerich, A. W. Dey, L. Samuelson, H. Bauer, K. Deppert, and A. Mikkelsen, Nano Lett. **10**, 4443 (2011).
[4] S. Breuer, C. Pfüller, T. Flissikowski, O. Brandt, H. T. Grahn, and H. Riechert, Nano Lett. **11**, 1276 (2011).
[5] T. Bryllert, L. E. Wernersson, T. Lowgren, and L. Samuelson, Nanotechnol. **17**, S227 (2006).
[6] M. T. Björk, B. J. Ohlsson, C. Thelander, A. I. Persson, K. Deppert, L. R. Wallenberg, and L. Samuelson, Appl. Phys. Lett. **81**, 4458 (2002).
[7] C. Gutsche, A. Lysov, D. Braam, I. Regolin, K. Keller, Z.-A. Li, M. Geller, M. Spasova, W. Prost, and F.-J. Tegude, Adv. Funct. Mater. **22**, 929 (2012).
[8] N. Sköld, L. S. Karlsson, M. W. Larsson, M. E. Pistol, W. Seifert, J. Tragardh, and L. Samuelson, Nano Lett. **5**, 943 (2005).
[9] H. J. Joyce, J. Wong-Leung, Q. Gao, H. Tan, and C. Jagadish, Nano Lett. **10**, 908 (2010).
[10] L. E. Fröberg, W. Seifert, and J. Johansson, Phys. Rev. B **76**, 153401 (2007).
[11] L. Jensen, M. Bjork, S. Jeppesen, A. Persson, B. Ohlsson, and L. Samuelson, Nano Lett. **4**, 1961 (2004).
[12] V. G. Dubrovskii, N. V. Sibirev, G. E. Cirlin, A. D. Bouravleuv, Y. B. Samsonenko, D. L. Dheeraj, H. L. Zhou, C. Sartel, J. C. Harmand, G. Patriarche *et al.*, Phys. Rev. B **80**, 205305 (2009).
[13] J. C. Harmand, F. Glas, and G. Patriarche, Phys. Rev. B **81**, 235436 (2010).
[14] P. Kratzer, S. Sakong, and V. Pankoke, Nano Lett. **12**, 943 (2012).
[15] N. N. Ŝeftal' and C. A. Magomedov, Kristall/ Technik **14**, 193 (1965).
[16] S. O. Mariager, C. M. Schlepütz, M. Aagesen, C. B. Sørensen, E. Johnson, P. R. Willmott, and R. Feidenhans'l, Phys. Status Solidi A **206**, 1771 (2009).
[17] S. O. Mariager, S. B. Sørensen, M. Aagesen, J. Nygård, P. R. Willmott, R. Feidenhans'l, and P. R. Willmott, Appl. Phys. Lett. **91**, 083106 (2007).
[18] K. A. Dick, P. Caroff, J. Bolinsson, M. E. Messing, J. Johansson, K. Deppert, R. L. Wallenberg, and L. Samuelson, Semicond. Sci. Technol. **25**, 024009 (2010).
[19] V. Pankoke, P. Kratzer, and S. Sakong, Phys. Rev. B **84**, 075455 (2011).
[20] N. Moll, A. Kley, E. Pehlke, and M. Scheffler, Phys. Rev. B **54**, 8844 (1996).
[21] R. Leitsmann and F. Bechstedt, J. Appl. Phys. **102**, 063528 (2007).
[22] G. Schwarz, Ph.D. thesis, TU Berlin, 2002, http://opus.kobv.de/tuberlin/volltexte/2002/407/
[23] J. N. Shapiro, A. Lin, D. L. Huffaker, and C. Ratsch, Phys. Rev. B **84**, 085322 (2011).
[24] C. T. Foxon, Acta Electronica **21**, 139 (1978).
[25] P. Kratzer and M. Scheffler, Phys. Rev. Lett. **88**, 036102 (2002).
[26] K. Seino, A. Ishii, and T. Aisaka, Surf. Sci. **438**, 43 (1999).
[27] K. Seino, A. Ishii, and T. Aisaka, Jpn. J. Appl. Phys. **39**, 4285 (2000).
[28] C. Heyn and M. Harsdorff, Phys. Rev. B **55**, 7034 (1997).
[29] G. Kresse and J. Hafner, Phys. Rev. B **47**, 558 (1993).
[30] P. E. Blöchl, Phys. Rev. B **50**, 17953 (1994).
[31] H. J. Monkhorst and J. D. Pack, Phys. Rev. B **13**, 5188 (1976).
[32] J. P. Perdew, K. Burke, and M. Ernzerhof, Phys. Rev. Lett. **77**, 3865 (1996).
[33] E. Penev, S. Stojković, P. Kratzer, and M. Scheffler, Phys. Rev. B **69**, 115335 (2004).
[34] C. Ratsch and M. Scheffler, Phys. Rev. B **58**, 13163 (1998).
[35] S. Horch, H. T. Lorensen, S. Helveg, E. Lægsgaard, I. Stensgaard, K. W. Jacobsen, J. K. Nørskov, and F. Besenbacher, Nature (London) **398**, 134 (1999).
[36] C. M. Haapamaki and R. R. LaPierre, Nanotechnol. **22**, 335602 (2011).
[37] V. G. Dubrovskii, N. Sibirev, R. A. Suris, G. E. Cirlin, J. C. Harmand, and V. M. Ustinov, Surf. Sci. **601**, 4395 (2007).
[38] V. G. Dubrovskii, G. E. Cirlin, I. P. Soshnikov, A. A. Tonkikh, N. V. Sibirev, Y. B. Samsonenko, and V. M. Ustinov, Phys. Rev. B **71**, 205325 (2005).
[39] J. C. Harmand, G. Patriarche, N. Péré-Laperne, M.-N. Mérat-Combes, L. Travers, and F. Glas, Appl. Phys. Lett. **87**, 203101 (2005).
[40] C. Sartel, D. L. Dheeraj, F. Jabeen, and J. C. Harmand, J. Cryst. Growth **312**, 2073 (2010).
[41] V. Jindal and F. Shahedipour-Sandvik, J. Appl. Phys. **107**, 054907 (2010).
[42] L. Lymperakis and J. Neugebauer, Phys. Rev. B **79**, 241308 (2009).
[43] V. Jindal and F. Shahedipour-Sandvik, J. Appl. Phys. **105**, 084902 (2009).
[44] T. Takebe, M. Fujii, T. Yamamoto, K. Fujita, and T. Watanabe, J. Appl. Phys. **81**, 7273 (1997).